RSC Advances

PAPER

View Article Online
View Journal | View Issue

Cite this: *RSC Adv.*, 2015, **5**, 29022

Synthesis, characterization, electrochemical properties and catalytic reactivity of *N*-heterocyclic carbene-containing diiron complexes†

Yanhong Wang,[ab] Tianyong Zhang,*[ab] Bin Li,*[ab] Shuang Jiang[ab] and Liao Sheng[ab]

Received 24th November 2014
Accepted 13th March 2015

DOI: 10.1039/c4ra15150j

www.rsc.org/advances

(μ-dmedt)[Fe(CO)$_3$]$_2$ (**I**, dmedt = 2,3-butanedithiol) was chosen as the parent complex. A series of new model complexes, *N*-heterocyclic carbene (NHC) substituted (μ-dmedt)[Fe–Fe]–NHC (**II**, (μ-dmedt)[Fe(CO)$_2$]$_2$[I$_{Me}$(CH$_2$)$_2$I$_{Me}$], I$_{Me}$ = 1-methylimidazol-2-ylidene; **III**, {(μ-dmedt)[Fe$_2$(CO)$_5$]}$_2$[I$_{Me}$(CH$_2$)$_2$I$_{Me}$]; **IV**, (μ-dmedt)[Fe$_2$(CO)$_5$]IMes, IMes = 1,3-bis(2,4,6-trimethylphenyl)imidazol-2-ylidene; **V**, (μ-dmedt)[Fe$_2$(CO)$_5$]IMe, IMe = 1,3-dimethylimidazol-2-ylidene) as mimics of the [Fe–Fe]–H$_2$ase active site were synthesized from **I** and characterized using solution IR spectroscopy, NMR spectroscopy, elemental analysis and single-crystal X-ray diffraction. The electrochemical properties of complexes **I–V**, with and without the addition of HOAc, were investigated by cyclic voltammetry in the coordinating solvent CH$_3$CN to evaluate the effects of different NHC ligands on the redox properties of the iron atoms of the series of complexes. It was concluded that all the new complexes are electrochemical catalysts for proton reduction to hydrogen. The symmetrically substituted cisoid basal/basal coordination complex **II** displays the most negative reduction potential owing to the stronger δ-donating ability of the NHC and the orientation of the NHC donor carbon as a result of the constraints of the bridging bidentate ligands. A new application for the [Fe–Fe]–NHC model complexes in the direct catalytic hydroxylation of benzene to phenol was also studied. Under the optimized experimental conditions (**II**, 0.01 mmol; benzene, 0.1 mL; CH$_3$CN, 2.0 mL; H$_2$O$_2$, 6.0 mmol; 60 °C, 3 h), the maximal phenol yield was 26.7%.

Introduction

Hydrogenase enzymes, which are found in a variety of microorganisms and can efficiently catalyze the reduction of protons to hydrogen, can be classified into [Fe]–H$_2$ases (Hmd H$_2$ases), [Ni–Fe]–H$_2$ases and [Fe–Fe]–H$_2$ases (H-cluster). Chemists are interested in studying the biomimetic chemistry of [Fe–Fe]–H$_2$ases as they have the highest and fastest catalytic capability for the production of hydrogen among the three classes.[1] Moreover, [Fe–Fe]–H$_2$ases are the most amenable to small molecule model studies because of their resemblance to well known organometallic complexes of the type (μ-SR)$_2$[Fe^{I}(CO)$_2$-L]$_2$.[2] To date, the diiron models (μ-pdt)[Fe(CO)$_3$]$_2$ (pdt = 1,3-propanedithiolato), (μ-edt)[Fe(CO)$_3$]$_2$ (edt = 1,2-ethanedithiolato), (μ-adt)[Fe(CO)$_3$]$_2$ (adt = 2-azapropane-1,3-dithiolato), (μ-odt)[Fe(CO)$_3$]$_2$ (odt = oxadithiolate) and (μ-tdt)[Fe(CO)$_3$]$_2$ (tdt = thiodithiolate), and their derivatives have been extensively studied both in terms of structure and functional mimics of the enzyme active site.

N-Heterocyclic carbenes (NHCs) are electronic, sterically tunable and stable with a range of transition metal complexes. NHCs can activate some bonds (C–H, C–C and C–N) at the N atom functionalities in the presence of transition metals.[3] Moreover, iron atoms combined with NHCs are more electron-rich and more easily accept protons for catalytic H$_2$ production due to the strong δ-electron-donating with negligible

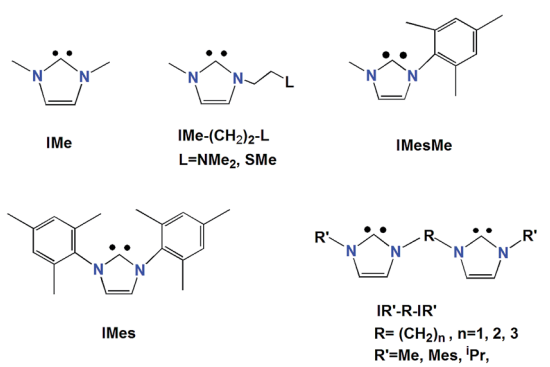

Fig. 1 The NHCs widely used in diiron model complexes.

[a]*School of Chemical Engineering and Technology, Tianjin Key Laboratory of Applied Catalysis Science and Technology, Tianjin University, Tianjin 300072, China. E-mail: tyzhang@tju.edu.cn; libin@tju.edu.cn*

[b]*Collaborative Innovation Center of Chemical Science and Engineering (Tianjin), Tianjin 300072, China*

† Electronic supplementary information (ESI) available. CCDC 1035522 (**II**) and 1035526 (**IV**), electrochemistry results and GC figures. For ESI and crystallographic data in CIF or other electronic format see DOI: 10.1039/c4ra15150j

π-electron-accepting ability and great potential of NHCs.[3b,4] The powerful ligands used for the design of diiron systems are listed in Fig. 1.[5]

Herein, we chose (μ-dmedt)[Fe(CO)$_3$]$_2$ (dmedt = 2,3-butanedithiol) as the parent complex due to its greater durability upon electrochemical cycling.[6] Donovan[6] synthesized complex **I** by the reaction of iron dodecacarbonyl with 2,3-butanedithiol. However, we used iron pentacarbonyl reacted with 2,3-butanedithiol to yield the same complex **I**.[7] Typical NHC ligands of IMe, IMes and $I_{Me}(CH_2)_2I_{Me}$ which are different to each other in structure were chosen to synthesise NHC-containing [Fe–Fe]–H_2ase models. The main aims of this study were: (i) to prepare the first NHC-containing [(μ-dmedt)Fe$_2$(CO)$_6$] models, both monosubstituted and disubstituted model complexes were included; (ii) to examine the influences of different NHC ligands upon the structures and properties of the NHC-containing complexes.

Iron complexes containing NHC ligands were first used as homogeneous catalysts in 2000 and have since become highly attractive.[8] Various organic transformations catalyzed by Fe–NHC have been achieved, including hydrosilylation reactions,[9] aryl Grignard–alkyl halide cross-coupling reactions,[10] Kumada-type alkyl–alkyl cross-coupling reactions[11] and ring-opening polymerization[12] *etc.* However, only [Fe–Fe]–NHC has been used for the reduction of protons to hydrogen until now.[13] In order to study the catalytic reactivity of [Fe–Fe]–NHC complexes, the direct hydroxylation of benzene to phenol *via* Scheme 1 by a series of NHC substituted diiron complexes in mild conditions was investigated.

Results and discussion

Synthesis and characterisation of the diiron complexes

The imidazolium salts $[I_{Me}(CH_2)_2I_{Me}]\cdot 2HBr$ (**1**), IMes·HCl (**2**) and IMe·HI (**3**), which are easily deliquescent white solids, were prepared with high yields as previously reported.[4a,14] The ethidene-bridged imidazolium salt $[I_{Me}(CH_2)_2I_{Me}]\cdot 2HBr$ was characterized by ^{1}H NMR and shows a singlet at 8.84 ppm for the protons of the two NC*H*N units in its two bridged imidazole rings.

The mono- and bi-NHC substituted complexes were synthesized by the facile reaction of the all-carbonyl complex **I** (Scheme 2) with the corresponding imidazolium salt and a strong base (*t*-BuOK) in THF at room temperature under sufficient stirring and monitored by solution IR spectroscopy. All the new model complexes could be handled in air and stored in atmospheric conditions for a couple of weeks, as both the solids and solutions of these complexes are relatively stable to air and water and are not hygroscopic.

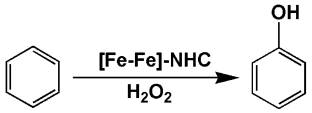

Scheme 1 Direct hydroxylation of benzene to phenol by [Fe–Fe]–NHC complexes.

The IR spectra of the five complexes displayed three or four absorption bands in the range 2073–1886 cm^{-1} (Fig. 2) for their terminal carbonyls in CH_2Cl_2. The bands of **II–V** were considerably shifted towards lower energy compared to those of their parent complex **I**, which is obviously due to their CO ligands being substituted by stronger electron-donating NHC ligands. Previous studies state that iron atoms become more electron-rich and more easily accept protons for catalytic H_2 production after the hexacarbonyl parent complex is substituted by stronger δ-donating ligands.[5b,15] As a result, stronger back-bonding from the metal to the CO ligands is formed, then the $\nu_{C=O}$ absorbance bands shift towards lower frequencies. So, we estimate that the $\nu_{C=O}$ bands can be considered as a useful indicator for evaluating the variation in the electron density of the Fe atoms. However, the electron donating capacity of the bidentate dimer $I_{Me}(CH_2)_2I_{Me}$ which connects to the two iron atoms of the [Fe–Fe] active center is obviously much higher than that of the monodentate dimers, IMes or IMe, mainly due to not only the presence of the more electronegative nitrogen atom in the latter two ligands, but also the orientation of the NHC donor carbon as a result of the constraints of the bridging bidentate ligands.

2 equiv. of the imidazolium salt **1** was reacted with 7.2 equiv. *t*-BuOK in THF at room temperature followed by treatment of the resulting mixture with 1 equiv. of the parent complex **I** to ensure the complex **I** completely transformed. The chelated bidentate NHC substituted model complex **II** and di-NHC ligand substituted **III** were afforded in low yields (Scheme 2) which were isolated after purification by aluminium oxide chromatography. However, no complex with a similar configuration to **II** was produced in the similar studies by Morvan[4c] and Song.[16] This demonstrates that the bridged dithiolate cofactors in (μ-dmedt)[Fe(CO)$_3$]$_2$, (μ-pdt)[Fe(CO)$_3$]$_2$ (pdt = 1,3-propanedithiolate) and [(μ-SCH$_2$)$_2$(Nbu-*t*)][Fe(CO)$_3$]$_2$ play a key role in the production of these two types of model complexes. The IR spectrum of **II** is very close to those reported for the bis-cyanide complex [(μ-pdt)Fe$_2$(CN)$_2$(CO)$_4$]$^{2-}$ (1965, 1924, 1884 cm^{-1}),[2b,17] but shifted to lower frequencies than those of the disubstituted IMe complex [(μ-pdt)Fe$_2$(CO)$_4$(IMe)$_2$] (1967, 1926, 1888 cm^{-1})[5a] and the bis-phosphine complex [(μ-pdt)Fe$_2$(CO)$_4$(PMe$_3$)$_2$] (1979, 1940, 1898 cm^{-1}).[18] These IR data demonstrate that the bidentate $I_{Me}(CH_2)_2I_{Me}$ ligand exhibits a better electron-donating ability relative to that of CN, IMe and PMe$_3$. In addition, the IR spectrum of **III** displays almost the same pattern in the carbonyl region at very similar frequencies to the mono-substituted complexes **IV** and **V**, which suggests that **III** is also a monosubstituted complex.[4c]

Although we tried our best, single crystals of complexes **III** and **V** suitable for X-ray detection were not achieved. The structures of complexes **II** and **IV** were confirmed by X-ray analyses of single crystals obtained from hexane–dichloromethane solutions at low temperature, and the selected bond lengths and angles are given in Tables 1 and 2. The Fe_2S_2 skeleton of the two complexes shares the well-known butterfly conformation in which each iron center adopts a distorted square–pyramidal coordination geometry. The two Fe atoms of complex **II** (Fig. 3) are bridged by a bi-NHC ligand with a

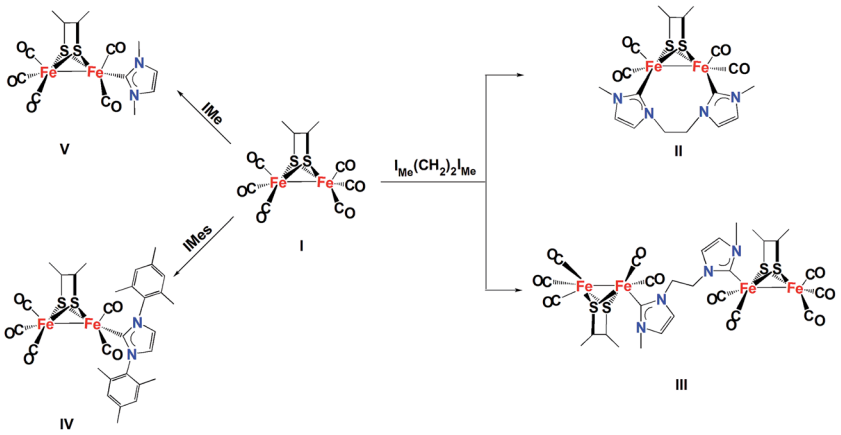

Scheme 2 Synthetic route of complexes II–V.

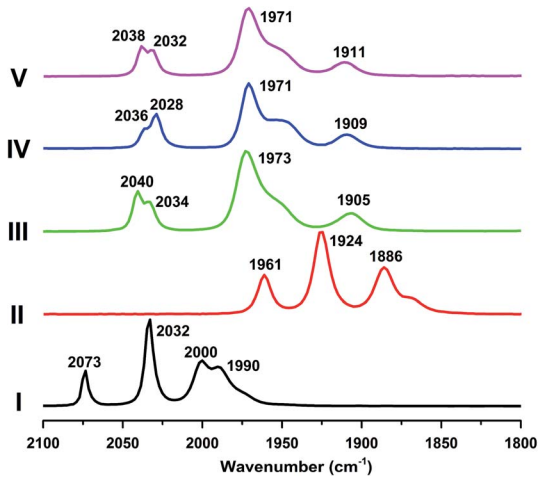

Fig. 2 The *v*(CO) region of the IR spectra of complexes I–V (observed in CH_2Cl_2 solution).

Table 1 Selected bond lengths (Å) for complexes II and IV

	II	IV
Fe(1)–Fe(2)	2.5952(6)	2.5870(12)
Fe(1)–S(1)	2.2474(8)	2.2450(18)
Fe(1)–S(2)	2.2503(8)	2.2510(19)
Fe(2)–S(1)	2.2471(8)	2.2504(17)
Fe(2)–S(2)	2.2381(8)	2.2452(19)
Fe(1)–C(1)	1.7490(3)	1.8000(8)
Fe(1)–C(8)	1.9910(3)	—
Fe(2)–C(5)	—	1.7540(7)
Fe(2)–C(10)	—	2.0000(6)
Fe(2)–C(13)	1.9690(3)	—

Table 2 Selected bond angles (Deg) for complexes II and IV

	II	IV
S(1)–Fe(1)–S(2)	79.36(3)	78.88(7)
S(1)–Fe(1)–Fe(2)	54.73(2)	54.97(5)
S(2)–Fe(1)–Fe(2)	54.46(2)	54.77(5)
S(2)–Fe(2)–S(1)	79.62(3)	78.89(7)
S(2)–Fe(2)–Fe(1)	54.90(19)	54.98(5)
S(1)–Fe(2)–Fe(1)	54.74(2)	54.77(5)
Fe(1)–S(1)–Fe(2)	70.54(2)	70.27(6)
Fe(1)–S(2)–Fe(2)	70.65(2)	70.25(6)
N(1)–C(10)–N(2)	—	101.90(5)
N(1)–C(8)–N(2)	103.10(2)	—
N(3)–C(13)–N(4)	103.70(2)	—
N(2)–C(9)–C(10)	115.80(2)	—
N(3)–C(10)–C(9)	113.90(3)	—

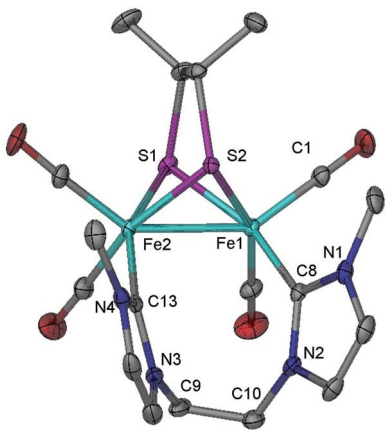

Fig. 3 X-ray crystal structure of complex II (ellipsoids at 30% probability level). The hydrogen atoms are omitted for clarity.

symmetrically chelated cisoid basal/basal coordination pattern and adopt a distorted square-pyramidal geometry. The Fe–Fe bond distance in **II** (2.5952(6) Å) is shorter than that of the same NHC substituted model complex **A** (Fig. 5) (2.6253(4) Å) made by Morvan,[4c] but is longer than that of complex **IV** (Fig. 4) (2.5870(12) Å). The Fe–C bond distances of the carbonyl of the {$Fe(CO)_2NHC$} subunits (**II**, 1.7490(3) Å; **IV**, 1.7540(7) Å) are significantly shorter than those of the carbonyl of the parent complex **I**, which are in the range 1.7887(19)–1.8090(2) Å.[7] This indicates an enhanced Fe–CO π-back-donation from the Fe

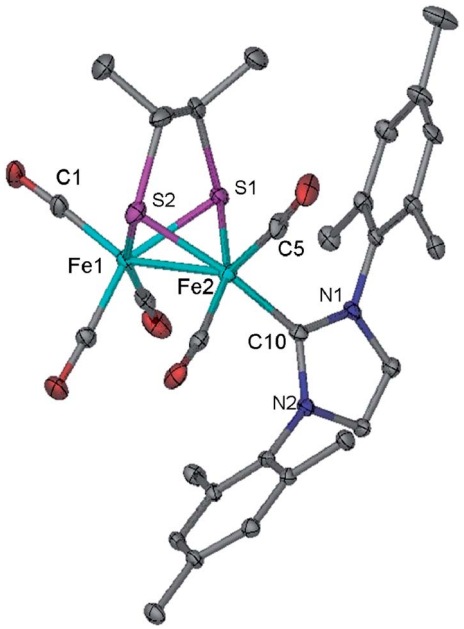

Fig. 4 X-ray crystal structure of complex IV (ellipsoids at 30% probability level). The hydrogen atoms are omitted for clarity.

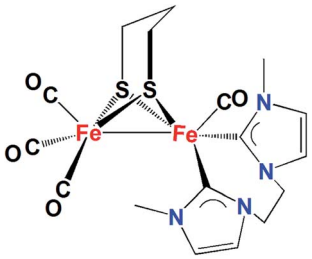

Fig. 5 Structure of complex A.

center to the $C_{carbene}$.[4b,19] The Fe–$C_{carbene}$ bond distances are typical of bonds having σ character.[4b,19] The Fe–$C_{carbene}$ bond lengths of **II** (1.991(3) Å, 1.969(3) Å) are shorter than that of complex **IV** (2.000(6) Å) owing to the relatively large space steric effect of the IMes ligand substituent.[5a]

Notably, in the crystal structure of complex **IV** (Fig. 4), the plane of the IMes ligand twists to a large extent to reduce steric interactions with the surrounding CO ligands. The IMes group in complex **IV** lies in a basal position in accordance with (μ-dmpdt)[Fe(CO)$_3$][Fe(CO)$_2$IMes] (ν_{CO} = 2030, 1971, 1947, 1913 cm^{-1}, in THF) and (μ-depdt)[Fe(CO)$_3$][Fe(CO)$_2$IMes] (ν_{CO} = 2025, 1971, 1946 and 1911 cm^{-1} in THF),[20] but in contrast with the apical positions of the same ligand in (μ-pdt)[Fe(CO)$_3$][Fe(CO)$_2$IMes] (ν_{CO} = 2035, 2027, 1969, 1947, 1916 cm^{-1}, in THF)[21] and (μ-odt)[Fe(CO)$_3$][Fe(CO)$_2$IMes] (ν_{CO} = 2039, 1969, 1947, 1924 cm^{-1}, in KBr).[16] It is probable that there is a strong steric repulsion between the IMes and dithiolate cofactor when the steric bulk is added to the bridgehead carbons of μ-SRS. But this different dithiolate cofactor does not drastically change the thiolate donor ability according to the IR data.

Cyclic voltammograms

The electrochemical properties of complexes **I–V**, with and without the addition of HOAc (acetic acid), were investigated by cyclic voltammetry (CV) in the coordinating solvent CH_3CN in the presence of Bu_4NPF_6 as the supporting electrolyte (Fig. 6). The redox potentials (referenced to Fc/Fc$^+$ = 0.00 V) of **I–V** are given in Table 3 and were assigned according to previous reports.[4c,21,22]

The hexacarbonyl parent **I** has quasi-reversible and irreversible reduction events at *ca.* −1.73 V and −2.23 V, respectively. It is obvious that the electrocatalysis occurs at the second reduction potential which corresponds to an Fe^0Fe^0 species in the presence of HOAc. The Fe^{II}–H^- species that results from the oxidative addition of a proton to Fe^0Fe^0 is set up to accept another proton, generating an (η^2-H_2)Fe^{II}–Fe^0 complex. This process is accounted for by an EECC (E = Electrochemical, C = Chemical) mechanism.[6,23]

However, a typical similar characteristic can be observed from the CVs that all members of the series display a two-electron reduction event at *ca.* −2.57, −2.14, −2.18 and −2.17 V, respectively. These events are shifted in a cathodic direction by *ca.* 860, 430, 470 and 460 mV for **II–V**, respectively, compared to the first reduction event of **I**. These shifts are consistent with the increase in electron density at the diiron centers as CO groups were replaced by the better electron donor of NHC ligands. Moreover, **II** appears at the most negative potentials among the known diiron complexes because the two basal CO groups of **I** have been substituted by the better electron donor ligand $I_{Me}(CH_2)_2I_{Me}$. The reduction potentials of **III**, **IV** and **V** under the CV conditions are very similar to each other, which is consistent with the similarity in electron density readily observed in the CO region of the IR spectra (Fig. 2). This suggests that the introduction of the bidentate NHC ligand bridged with two Fe atoms exerts a stronger influence on the redox potentials of the diiron complexes than the introduction of a monodentate carbene.

A quasi-reversible two-electron reduction $Fe^IFe^I \rightarrow Fe^0Fe^0$ couple at *ca.* −2.14 and −2.17 V was observed in the CVs of complexes **III** and **V**, respectively.[5b,21] Interestingly, for **III** and **V**, in the presence of HOAc, new reduction peaks were observed at the more negative peaks *ca.* −2.25 and −2.43 V when detected under N_2, but were not observed when the CV measurement of **V** was carried out under CO (Fig. S6†). So we suppose that the additional reduction events under N_2 can be attributed to the Fe^IFe^I/Fe^0Fe^0 couple of a coordinated solvent substituted species ((μ-dmedt)[Fe–Fe](NCCH$_3$)) which is likely to result from a radical chain reaction initiated by the production of the radical anion process,[1b,3a,23c,23d] not because the two-electron reduction process divided into two one-electron reduction processes. Moreover, the process of CO dissociation from the labile Fe^0Fe^0 radical anion was inhibited during the measurement in a CO saturated solution.[5a] The current heights of the first reduction peaks of **III** and **V** at *ca.* −2.07 and −2.17 V showed a slight increase with added increments of HOAc, while the second new reduction peaks showed a significant electrocatalytic response, which is typical of an electrocatalytic

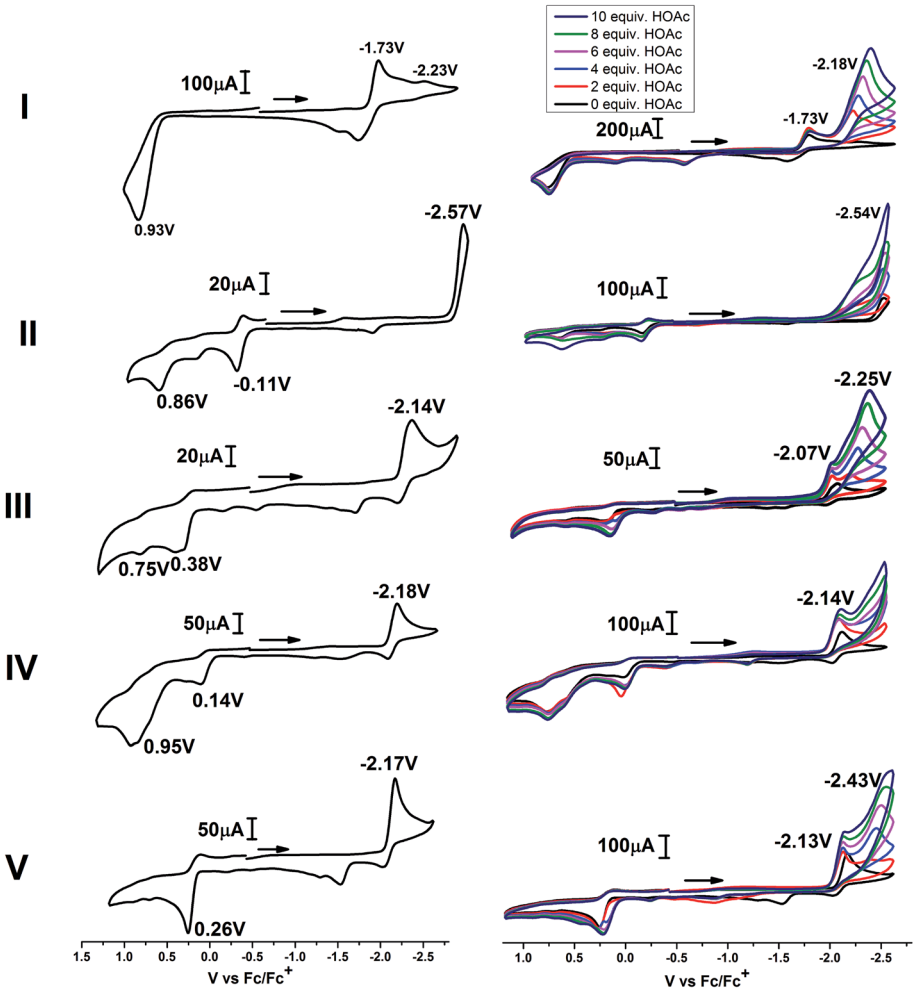

Fig. 6 Cyclic voltammograms of the complexes with and without HOAc (2, 4, 6, 8 and 10 equiv.) in CH_3CN solution (0.1 M n-Bu_4NPF_6) under N_2 at room temperature: (a) **I**, 2 mM, scan rate, 200 mV s^{-1}; (b) **II**, 2 mM, scan rate, 100 mV s^{-1}; (c) **III**, 1 mM (poor solubility), scan rate, 100 mV s^{-1}; (d) **IV**, 2 mM, scan rate, 200 mV s^{-1}; and (e) **V**, 2 mM, scan rate, 200 mV s^{-1}. All potentials are scaled to $Fc/Fc^+ = 0.00$ V.

process. This suggests that both the Fe^0Fe^0 and [(μ-dmedt)[Fe–Fe](NCCH$_3$)] species can combine with protons and be active toward electrocatalytic H_2 production, but the reactivity of the latter is stronger than that of the former.

The conjunction of the Fe and IMes ligand valence orbital permits the uptake of two electrons at the same potential. What's more, in addition to a one-electron Fe–Fe reduction, DFT shows that the aryl-substituted NHC can accept a second electron more readily than the Fe–Fe manifold.[16,22b] The CV of **IV** shows that the two electron process of electrocatalytic H_2 production (one electron at the Fe–Fe center and one electron on the IMes ligand) with a quasi-reversible reduction at *ca.* −2.18 V can be assigned to the $Fe^IFe^I(IMes)^0 \rightarrow Fe^0Fe^I(IMes)^{-1}$ reduction. In the presence of HOAc, the Fe^0 of the $[Fe^0$–$Fe^I(IMes)^{-1}]^{2-}$ species is protonated to afford the Fe–H species of the monoanion $[Fe^{II}(H)$–$Fe^I(IMes)^{-1}]^-$. A second protonation

Table 3 Redox potentials of complexes **I**–**V**

Complex	E_{pc}/V *vs.* Fc/Fc^+, E: $Fe^IFe^I \rightarrow Fe^0Fe^0$	E_{pc}/V *vs.* Fc/Fc^+, $Fe^IFe^I \rightarrow Fe^{II}Fe^I$, $Fe^{II}Fe^I \rightarrow Fe^{II}Fe^{II}$
I	−1.73[a], −2.23[b]	0.93, —
II	−2.57	−0.11, 0.86
III	−2.14	0.38, 0.75
IV	−2.18[c]	0.14, 0.95
V	−2.17	0.28, 0.71

[a] E_1: $Fe^IFe^I \rightarrow Fe^0Fe^I$. [b] E_2: $Fe^0Fe^I \rightarrow Fe^0Fe^0$. [c] $Fe^IFe^I(IMes)^0 \rightarrow Fe^0Fe^I(IMes)^{-1}$.

and internal electron transfer from the reduced IMes ligand to the iron center result in the release of dihydrogen and regeneration of the $Fe^{I}Fe^{I}$ starting material. On the basis of previous reports, the electrochemical process of **IV** is also inferred as an EECC mechanism.[4c,16,21]

In the presence of HOAc, the current heights of the single cathodic events in the CVs of the five complexes almost increase linearly with the concentration of HOAc (Fig. S8†). The steeper slope displayed by the line of current–concentration indicates greater sensitivity to acid concentration. That is to say electrocatalytic reactions occurred.[23c,23d]

Catalytic hydroxylation

Our previous study indicated that the Fe–Fe bond in a complex with an electron-donating ligand could be oxidized more easily by H_2O_2 to form an oxygen-transfer intermediate.[7] Therefore, the better electron-donating NHC ligand substituted diiron model complexes were used as catalysts for the hydroxylation of benzene.

Hydroxylation of benzene with H_2O_2 (30%, w/w, in H_2O) was carried out in a 25 mL round bottom flask equipped with a reflux condenser and a magnetic stirrer. All the experiments were conducted at ambient pressure. Blank controls (without catalyst or H_2O_2) were also conducted, and no phenol was detected.

At first, different oxidants (O_2, H_2O_2, PhIO, and *m*-CPBA) were used as hydroxylation reagents (Table 4). The phenol yield with H_2O_2 was more than twice that with *m*-CPBA under the same conditions. However, O_2 and PhIO were not able to oxidize benzene to phenol under the given experimental conditions. Thus, H_2O_2 was chosen as the oxidant in the following hydroxylation. Some parameters which would affect the phenol yield such as reaction time, temperature, amount of catalyst and H_2O_2 were also investigated (Fig. S9†). The temperature had a strong effect on the phenol yield. The reaction rate increased with temperature increments up to 60 °C, leading to an increased phenol yield. However, the phenol yield decreased with further increase of the temperature, which is probably partly attributable to side reactions (Fig. S11†). Due to the complexity of the oxidation reactions, it is hard to identify all the by-products. Especially as some of the by-products could probably not be detected under the special GC analytical conditions. In the presence of 0.01 mmol of catalyst and 1 mmol of benzene – *i.e.* 100 equivalents of benzene – a yield of 25% phenol was obtained. This means that 1 molecule of catalyst produced 25 molecules of product, which provides evidence for a catalytic process. However, adding more catalyst did not change the yield of phenol obviously, only increased the rate. It is possible that the reaction is indiscriminate and gives several oxidized products of which phenol is just one (possibly the other oxidized products have very high retention times and are not detected by GC). Fig. S9† illustrates that under the optimized experimental conditions (**IV**, 0.01 mmol; benzene, 0.1 mL; CH_3CN, 2.0 mL; H_2O_2, 6.0 mmol; 60 °C; 3 h), the maximal phenol yield was 25.9%.

Complex **I** and its NHC ligand substituted derivatives were used as homogeneous catalysts to catalyze the hydroxylation of benzene with H_2O_2, and phenol was detected as the main product in all the reactions (Table 5). Although there were small differences in the yields of phenol, they are consistent with the first oxidation events presumed to be $Fe^{I}Fe^{I}/Fe^{II}Fe^{I}$ for **I–V** which are at *ca.* 0.93 V, −0.11 V, 0.38 V, 0.14 V and 0.28 V respectively as shown in the CVs (Fig. 6). From the infrared spectra (Fig. 2) we can observe the ν_{CO} of complexes **III**, **IV** and **V** are little different due to the similar electron densities of Fe–Fe, which should be consistent with their almost similar activity for the hydroxylation of benzene. It is notable that, for complex **II**, the bridging ligand $[I_{Me}(CH_2)_2I_{Me}]$ reduced the flexibility of the diiron complex and hindered the rotation of the subunits which against H_2O_2 attack Fe–Fe bond to form the oxygen-transfer intermediate.[24] On the other hand, although the increasing electron donor effect due to the disubstituted ligands should enhance its catalytic ability, the effect of the steric hindrance of the bridging ligands overcomes the electron donor effect. Therefore, the yield of phenol catalyzed by complex **II** increased little.

To our surprise, for the hydroxylation of benzene to phenol with *m*-CPBA by $FeSO_4$ no phenol was detected by gas chromatography (GC) under the same experimental conditions (Table 5 and Fig. S12†). Therefore, we inferred that the mechanism of hydroxyl radical oxidation for the hydroxylation of benzene to phenol may be ruled out here. DFT calculations carried out by Darensbourg[24] state that the iron-based oxygenated product Fe^{II}-(**μ-O**)-Fe^{II} is more stable than the S-oxygenated product; this indicates that the Fe^{II}-(**μ-O**)-Fe^{II} isomer is thermodynamically favored in the diiron model complexes. Hence, we infer that the Fe^{II}-(**μ-O**)-Fe^{II} active intermediate may be more

Table 4 Effects of different oxidants on the hydroxylation of benzene to phenol[a]

Entry	Catalyst	Oxidant	Yield (%)
1	**IV**	H_2O_2	25.9
2	**IV**	*m*-CPBA	12.1
3	**IV**	PhIO	0
4	**IV**	O_2	0

[a] Catalyst, 0.01 mmol; benzene, 0.1 mL; CH_3CN, 2.0 mL; oxidant, 6.0 mmol; 60 °C; 3 h.

Table 5 Effects of different catalysts and oxidants on the hydroxylation of benzene to phenol[a]

Entry	Catalyst	Catalyst (mmol)	Oxidant	Yield (%)
5	**I**	0.05	H_2O_2	7.5[7]
6	**I**	0.01	H_2O_2	0
7	**II**	0.01	H_2O_2	26.7
8	**III**	0.01	H_2O_2	23.4
9	**V**	0.01	H_2O_2	24.3
10	$FeSO_4$	0.01	*m*-CPBA	0

[a] Catalyst; benzene, 0.1 mL; CH_3CN, 2.0 mL; oxidant 6.0 mmol; 60 °C; 3 h.

likely to be capable of transferring an oxygen atom to the aromatic substrate in the hydroxylation process. Although the isolation of the Fe^{II}-(**μ-O**)-Fe^{II} species based on our diiron complexes has not been achieved to date, the Fe-(**μ-O**)-Fe sites in Fe/ZSM-35 as the oxygen transfer species in the catalytic oxidation has been identified by C. Li's group using *in situ* resonance Raman spectroscopy.[25] A mechanism for the hydroxylation of benzene was proposed based on the theoretical and experimental results in our previous work,[7] which suggests that the reaction involves an electrophilic addition process between the Fe^{II}-(**μ-O**)-Fe^{II} species and the benzene substrate. Combined with the electrophilic addition process, a further hydrogen-atom shift occurs, and then the oxygen atom is transferred to the substrate.

Conclusions

Four new monodentate and bidentate NHC-containing iron complexes (**II–V**) were synthesized by facile carbonyl replacement on the parent complex **I** in THF at room temperature. The X-ray crystallography results revealed that the monodentate NHC ligand in **IV** is coordinated to one of the two Fe atoms and located in a basal position. Whereas, the chelated bidentate ligand $I_{Me}(CH_2)_2I_{Me}$ in **II** is connected to the two Fe atoms with a symmetrically substituted cisoid basal/basal coordination pattern. It is worth pointing out that all of the four complexes were found to be catalysts for proton reduction to hydrogen under electrochemical conditions and the results confirmed that the more δ-donating of NHC, the easier the reduction. The reduction potential of the novel model complex **II** at *ca.* −2.57 V is more negative than the other diiron complexes we have known. The electrocatalytic mechanism for the proton reduction to H_2 by [Fe–Fe]–NHC will be investigated in our further studies. In addition, the abilities of these complexes to act as homogeneous catalysts for the hydroxylation of benzene to phenol (with a maximum phenol yield of 26.7%) were correlated with the initial potentials of their oxidation events.

Experimental section

General comments

Some reactions and operations were carried out using standard Schlenk and vacuum-line techniques under a nitrogen atmosphere. All solvents and reagents were purchased from Guangfu Chemical and Sigma-Aldrich, respectively. $Fe(CO)_5$ was obtained as a gift from Jiangsu Tianyi Ultra-fine Metal Powder Co., Ltd (China). Solvents were dried and distilled prior to use according to the standard methods. The purified solvents were stored with molecular sieves under N_2 for no more than 1 week before use. THF, hexane, CH_2Cl_2, toluene and acetonitrile were stirred over molecular sieves under N_2 for 24 h prior to further purification. THF and hexane were distilled from sodium/benzophenone. Acetonitrile was distilled from NaH. All the solvents were deoxygenated before every use.

The NMR spectra were measured on a Bruker AVANCE III 400 MHz NMR spectrometer. ^{1}H NMR and ^{13}C NMR shifts were referenced to residual solvent resonances according to literature values. Solution IR spectra were recorded on a Shimadzu FTIR-8400 spectrometer using 0.1 mm KBr sealed cells. Elemental analysis was carried out on a Heraeus CHN-Rapid, fully automatic elemental analyzer with TCD detection, type: TMT CHN, BESTELL-NR 2215001.

Preparation of $I_{Me}(CH_2)_2I_{Me}\cdot 2HBr$ (1)

A solution of 1-methylimidazole (2.49 g, 30 mmol) and 1,2-dibromoethane (2.82 g, 15 mmol) in CH_3CN (20 mL) was refluxed for 72 h under a nitrogen atmosphere. The precipitate was filtered after cooling through a double-ended needle, and washed with THF (3 × 10 mL). Following drying *in vacuo*, product **1** was obtained as a white, hygroscopic powder (4.96 g, 93.9%). The bromide salt must be stored under a nitrogen atmosphere in a dryer due to its easy deliquescence. ^{1}H NMR (400 MHz, D_2O): δ = 3.962 ($2CH_3$–), 4.825 (–CH_2CH_2–), 7.501 ($2CH_3NCH$═CHN), 7.562 ($2CH_3NCH$═CHN), 8.840 (2NCHN).

Preparation of IMes·HCl (2)

Glyoxylaldehyde (40%, 6.27 g, 43.21 mmol) and 50 mL anhydrous alcohol were added dropwise over 1 h to an anhydrous alcohol (50 mL) solution of 2,4,6-trimethylaniline (4.63 g, 33.57 mmol). The mixture was stirred at room temperature for 12 h and then a yellow solid was separated out; the insoluble material was filtered and then washed with cold alcohol. After drying in a vacuum, 3.01 g of the yellow solid of *N*,*N*′-(ethane-1,2-diylidene) bis(2,4,6-trimeth-ylaniline) (imine) in 61.5% yield was achieved.

In a flask, the above imine (1.50 g, 5.13 mmol) was dissolved in THF (12.5 mL), followed by the dropwise addition of chloromethyl ethyl ether (0.612 g, 6.15 mmol). Then, the mixture was stirred under N_2 at 40 °C for 18 h. The precipitate was filtered after cooling, and washed with ethyl ether (2 × 20 mL). The residue was dissolved in as little anhydrous alcohol as possible, and then ethyl ether (25 mL) was added to the extract. The above operation was repeated until a white solid was obtained. The white solid was dried under vacuum to afford salt **2** (0.95 g, 54.1%).

Preparation of IMe·HI (3)

Methylimidazole (10.2 g, 0.125 mol) and iodomethane (17.8 g, 0.125 mol) were dissolved in 100 mL toluene and stirred at reflux for 12 h under an nitrogen atmosphere. After cooling to room temperature toluene was filtered off through a double-ended needle then a white solid was formed. The residue was dissolved in as little anhydrous alcohol as possible, and then ethyl ether (50 mL) was added to the extract. The above operation was repeated until a white solid was obtained. The white solid was dried *in vacuo* to yield 27.2 g (97.1%) of **3**. The same as $I_{Me}(CH_2)_2I_{Me}\cdot 2HBr$, IMe·HI must be stored under a nitrogen atmosphere in a dryer.

Preparation of (μ-dmedt)$Fe_2(CO)_6$ (I)

$Fe(CO)_5$ (13.4 g, 68.6 mmol) and 2,3-butanedithiol (2.77 g, 22.7 mmol) were added to 55 mL toluene and stirred at reflux for

29 h under a nitrogen atmosphere. Then, the solvent was distilled under 140 °C, and the residue was dissolved in a little toluene and loaded onto a silica gel column. The product was then eluted with hexane. The solvent was evaporated from the dark red eluant to yield **I** as a red powder (3.439 g, 37.9%). IR (CH_2Cl_2) ν_{CO} = 2073, 2032, 2000, 1990 cm^{-1}. ^1H NMR (400 MHz, $CDCl_3$) δ = 2.24(s, C*H*═C*H*), 1.36(m, CH_3C–CCH_3). ^{13}C NMR (400 MHz, $CDCl_3$) δ = 208.63 (*C*O); 55.21 and 49.37 (S*C*H(CH_3)CH(CH_3)*C*HS); 20.61 and 19.14 (SCH(*C*H_3)CH(*C*H_3)CHS). Elemental analysis: calc. for $C_{10}H_8O_6Fe_2S_2$: C, 30.03; H, 2.02. Found: C, 30.11; H, 2.01.

Preparation of (μ-dmedt)$Fe_2(CO)_4(I_{Me}(CH_2)_2I_{Me})$ (II) and [(μ-dmedt)$Fe_2(CO)_5]_2$ ($I_{Me}(CH_2)_2I_{Me}$) (III)

$I_{Me}(CH_2)_2I_{Me}$·2HBr (160 mg, 0.46 mmol) was dried *in vacuo* under N_2 for 30 min in a 50 mL Schenk flask, then *t*-BuOK (184 mg, 1.64 mmol) and THF (7 mL) were added to the mixture after dried *in vacuo* under N_2 for 20 min. After 3 h of vigorous stirring at room temperature, a THF (7 mL) solution of **I** (77 mg, 0.23 mmol) was transferred to the reaction mixture over 35 min by a double-ended needle at room temperature. The resulting mixture was stirred at room temperature for 1.25 h, and monitored by IR spectroscopy to confirm that the reaction had reached completion. The solution was evaporated to dryness *in vacuo*. The resulting red solid was dissolved in a minimum amount of CH_2Cl_2 and applied to an aluminium oxide column. The first red band was eluted with a CH_2Cl_2–hexane (1/2) mixture. Slow evaporation of the solvent gave **III** as an orange powder (26 mg, 29.0%). A second red band eluted with CH_2Cl_2–hexane (1/1) gave complex **II** as a red powder (11 mg, 12.4%) after slow evaporation of the solvents.

Complex II. IR (CH_2Cl_2) ν_{CO} = 1961, 1924, 1886 cm^{-1}. ^1H NMR (400 MHz, acetone-d_6) δ = 7.11–6.98 (m, 2 NC*H*═C*H*N), 5.85–5.43 (m, NCH_2CH_2N), 4.29 (m, NCH$_2$CH_2N), 3.95 (d, 2 NCH_3), 2.29 (m, SC*H*(CH_3)CH(CH_3)S), 1.94 (m, SCH(CH_3)C*H*(CH_3)S), 1.47 (d, SCH(CH_3)CH(CH_3)S), 1.26 (d, SCH(CH_3)CH(CH_3)S). ^{13}C NMR (400 MHz, acetone-d_6) δ = 222.32, 221.61 and 216.47 (*C*O); 188.95 ($C_{carbene}$); 123.76, 123.40, 122.98 and 122.06 (N*C*H═*C*HN); 54.90 and 54.57 (N*C*H$_2$*C*H$_2$N); 47.10 and 46,49 (N*C*H_3); 39.09 and 38.85 (S*C*H(CH_3)CH(CH_3)*C*HS); 20.70 and 20.35 (SCH(*C*H_3)CH(*C*H_3)CHS). Elemental analysis: calc. for $C_{18}H_{22}O_4N_2Fe_2S_2$: C, 40.47; H, 4.15; N, 10.49. Found: C, 40.34; H, 4.14; N, 10.52.

Complex III. IR (CH_2Cl_2) ν_{CO} = 2040, 2034, 1973, 1905 cm^{-1}. ^1H NMR (400 MHz, CD_2Cl_2) δ = 7.11 (m, 2 NC*H*═C*H*N), 6.24 (m, NCH_2CH_2N), 4.05 (d, 2 NCH_3), 2.06 (m, SC*H*(CH_3)C*H*(CH_3)S), 0.92 (d, SCH(CH_3)CH(CH_3)S). Elemental analysis: calc. for $C_{28}H_{30}O_{10}N_4Fe_4S_4$: C, 36.00; H, 3.24; N, 6.00. Found: C, 36.12; H, 3.23; N, 6.01.

Preparation of (μ-dmedt)$Fe_2(CO)_5$(IMes) (IV)

Solid **I** (93 mg, 0.23 mmol) and salt **2** (198 mg, 0.58 mmol) were combined, dried *in vacuo* for 30 min and then dissolved in THF (4.5 mL). After stirring for another 30 min, previously dried *t*-BuOK (130 mg, 1.16 mmol) in 3.5 mL of THF was added, and the resulting mixture was stirred for an additional 30 min, and monitored by IR spectroscopy to confirm that the reaction had reached completion. The solvent was then removed, and the red residue was dissolved in CH_2Cl_2 and loaded onto a silica gel column. Elution with petroleum ether removed the excess starting material **I**. The product was then eluted with CH_2Cl_2. The solvent was evaporated from the dark red eluant to yield product **IV** (140 mg, 89%). IR (CH_2Cl_2) ν_{CO} = 2036, 2028, 1971, 1909 cm^{-1}. ^1H NMR (400 MHz, acetone-d_6) δ = 7.46 and 7.36 (s, NC*H*═C*H*N); 7.08 and 7.06 (d, Ar*H*); 2.35 (s, *p*-ArCH_3); 2.21–2.16 (m, *o*-ArCH_3); 1.79 (m, SC*H*(CH_3)C*H*(CH_3)S); 1.04–0.92 (m, SCH(CH_3)CH(CH_3)S). ^{13}C NMR (400 MHz, acetone-d_6) δ = 216.02, 212.43 and 211.88 (*C*O); 187.48 ($C_{carbene}$); 138.99, 137.93, 136.06 (C_6H_2); 128.94 and 125.65 (N*C*H═*C*HN); 53.58 and 47.65 (S*C*H(CH_3)CH(CH_3)*C*HS); 20.23, 19.89, 19.43, 18.42, 18.14, 18.03 and 17.83 (CH_3). Elemental analysis: calc. for $C_{30}H_{32}O_5N_2Fe_2S_2$: C, 53.27; H, 4.78; N, 4.14. Found: C, 53.13; H, 4.79; N, 4.15.

Preparation of (μ-dmedt)$Fe_2(CO)_5$(IMe) (V)

Complex **V** was prepared by a procedure similar to that of **IV** from IMe·HI (585 mg, 2.61 mmol), **I** (1.00 g, 2.50 mmol) and *t*-BuOK (569 mg, 5.07 mmol). The product was obtained as an orange solid: yield 1.01 g, 86.1%. IR (CH_2Cl_2) ν_{CO} = 2038, 2032, 1971, 1911 cm^{-1}. ^1H NMR (400 MHz, CD_3CN) δ = 7.14 (s, NC*H*═C*H*N); 3.94 (s, NCH_3); 2.03 (s, SC*H*(CH_3)CH(CH_3)S), 1.23 (m, broad, SCH(CH_3)CH(CH_3)S), 0.88 (s, broad, SCH(CH_3)C*H*(CH_3)S). ^{13}C NMR (400 MHz, CD_3CN) δ = 217.40 and 212.08 (*C*O); 163.52 ($C_{carbene}$); 124.07 and 120.01 (N*C*H═*C*HN); 55.11 (N*C*H_3); 39.16 (S*C*H(CH_3)CH(CH_3)*C*HS); 20.07 (CH_3). Elemental analysis: calc. for $C_{14}H_{16}O_5N_2Fe_2S_2$: C, 35.92; H, 3.45; N, 5.98. Found: C, 36.02; H, 3.46; N, 5.96.

X-ray crystallography

The single-crystal X-ray diffraction data were collected with a Rigaku MM-007 diffractometer equipped with a Saturn 724CCD. Data were collected at 293 K or 113 K using a confocal monochromator with Mo-Kα radiation (λ = 0.71073 Å). Data collection, reduction and absorption correction were performed using the CRYSTALCLEAR program.[26] The structures were solved by direct methods using the SHELXS-97 program[27] and refined by the full-matrix least-squares technique (SHELXL-97)[28] on F^2. Hydrogen atoms were located by geometrical calculation. Details of crystal data, data collection and structure refinements are summarized in Table S1 and Fig. S1–S3.†

Cyclic voltammograms

Cyclic voltammograms were obtained in a three-electrode cell under N_2 using a CHI 660B electrochemical workstation. The working electrode was a glassy carbon disk (diameter 3 mm) polished with 3 and 1 μm diamond pastes and sonicated in ion-free water for 20 min prior to use. The reference electrode was a non-aqueous Ag/Ag^+ (in a CH_3CN solution of 0.01 M $AgNO_3$/0.1 M *n*-Bu_4NPF_6) electrode and the counter electrode was platinum wire. A solution of 0.1 M *n*-Bu_4NPF_6 in CH_3CN was used as the supporting electrolyte, which was degassed by bubbling with dry N_2 for 10 min before the measurements. Ferrocene was used as an internal standard under the same measuring conditions

and all potentials were referenced to the $Cp_2Fe^+/0$ couple at 0 V. During the electrocatalytic experiments under N_2, increments of glacial HOAc (chromatographic grade, ≧99.8%, water 0.15%, by the Karl Fischer method) were added by microsyringe.

Catalytic hydroxylation

Hydroxylation of benzene with H_2O_2 (30%, w/w, in H_2O) was carried out in a 25 mL round bottom flask equipped with a reflux condenser and a magnetic stirrer. In a typical reaction, **IV** (7 mg, 0.01 mmol) was dissolved in CH_3CN (2.0 mL). After the mixture was heated to the desired temperature, benzene (0.1 mL, 1.1 mmol) was added to the mixture. Lastly, a certain amount of H_2O_2 was added to start the reaction and the mixture was stirred for several hours. All the experiments were conducted at ambient pressure. Measurements of GC (9890B) equipped with a FID detector and a capillary column (OV-1701; 30 m × 0.25 mm × 0.25 μm) were performed to analyze the product mixture. The internal standard method was used for quantitative analysis and chlorobenzene was chosen as the internal standard substance. TPD analysis was carried out, from 80 °C to 200 °C at a ramp of 10 °C, then from 200 °C to 280 °C at a ramp of 30 °C. This reaction system appeared to have a high selectivity since phenol was the only product detected by GC.

Acknowledgements

We are grateful to the National Natural Science Foundation of China (21103121 and 21276187), the Research Fund for the Doctoral Program of Higher Education of China (20110032120011) and the Tianjin Municipal Natural Science Foundation (13JCQNJC05800) for financial support of this work.

References

1 (*a*) Z. Xiao, Z. Wei, L. Long, Y. Wang, D. J. Evans and X. Liu, *Dalton Trans.*, 2011, **40**, 4291–4299; (*b*) P. Li, M. Wang, C. He, G. Li, X. Liu, C. Chen, B. Åkermark and L. Sun, *Eur. J. Inorg. Chem.*, 2005, 2506–2513; (*c*) B.-E. Jugder, J. Welch, K.-F. Aguey-Zinsou and C. P. Marquis, *RSC Adv.*, 2013, **3**, 8142–8159.

2 (*a*) E. J. Lyon, I. P. Georgakaki, J. H. Reibenspies and M. Y. Darensbourg, *Angew. Chem., Int. Ed.*, 1999, **38**, 3178–3180; (*b*) A. L. Cloirec, S. P. Best, S. Borg, S. C. Davies, D. J. Evans, D. L. Hughesa and C. J. Pickett, *Chem. Commun.*, 1999, 2285–2286.

3 (*a*) R. Lopes, J. M. S. Cardoso, L. Postigo and B. Royo, *Catal. Lett.*, 2013, **143**, 1061–1066; (*b*) C. Tard and C. J. Pickett, *Chem. Rev.*, 2009, **109**, 2245–2274; (*c*) C. Cao, Y. Zhuang, J. Zhao, H. Liu, P. Geng, G. Pang and Y. Shi, *Synth. Commun.*, 2012, **42**, 380–387; (*d*) M. Lee, Z. Niu, D. V. Schoonover, C. Slebodnick and H. W. Gibson, *Tetrahedron*, 2010, **66**, 7077–7082.

4 (*a*) F. Godoy, C. Segarra, M. Poyatos and E. Peris, *Organometallics*, 2011, **30**, 684–688; (*b*) D. Morvan, J. F. Capon, F. Gloaguen, G. A. Le, M. Marchivie, F. Michaud, P. Schollhammer, J. Talarmin, J. J. Yaouanc, R. Pichon and N. Kervarec, *Organometallics*, 2007, **26**, 2042–2052; (*c*) L. Mercs, G. Labat, A. Neels, A. Ehlers and M. Albrecht, *Organometallics*, 2006, **25**, 5648–5656; (*d*) J. F. Capon, S. E. Hassnaoui, F. Gloaguen, P. Schollhammer and J. Talarmin, *Organometallics*, 2005, **24**, 2020–2022.

5 (*a*) C. M. Thomas, T. Liu, M. B. Hall and M. Y. Darensbourg, *Inorg. Chem.*, 2008, **47**, 7009–7024; (*b*) J. Wu, W. Dai, J. H. Farnaby, N. Hazari, J. J. Le Roy, V. Mereacre, M. Murugesu, A. K. Powell and M. K. Takase, *Dalton Trans.*, 2013, **42**, 7404–7413; (*c*) X. Wang, Z. Mo, J. Xiao and L. Deng, *Inorg. Chem.*, 2013, **52**, 59–65; (*d*) M. J. Ingleson and R. A. Layfield, *Chem. Commun.*, 2012, **48**, 3579–3589; (*e*) S. Zlatogorsky, C. A. Muryn, F. Tuna, D. J. Evans and M. J. Ingleson, *Organometallics*, 2011, **30**, 4974–4982.

6 E. S. Donovan, G. S. Nichol and G. A. N. Felton, *J. Organomet. Chem.*, 2013, **726**, 9–13.

7 X. Wang, T. Y. Zhang, Q. S. Yang, S. Jiang and B. Li, *Eur. J. Inorg. Chem.*, 2015, 817–825.

8 J. Louie and R. H. Grubbs, *Chem. Commun.*, 2000, 1479–1480.

9 (*a*) A. Volkov, E. Buitrago and H. Adolfsson, *Eur. J. Org. Chem.*, 2013, **11**, 2066–2070; (*b*) S. Demir, Y. Gökçe, N. Kaloğlu, J. B. Sortais, C. Darcel and İ. Özdemir, *Appl. Organomet. Chem.*, 2013, **27**, 459–464; (*c*) T. Hashimoto, S. Urban, R. Hoshino, Y. Ohki, K. Tatsumi and F. Glorius, *Organometallics*, 2012, **31**, 4474–4479; (*d*) D. Bézier, G. T. Venkanna, J. B. Sortais and C. Darcel, *ChemCatChem*, 2011, **3**, 1747–1750.

10 (*a*) C. Pranckevicius and D. W. Stephan, *Organometallics*, 2013, **32**, 2693–2697; (*b*) T. Hatakeyama, S. Hashimoto, K. Ishizuka and M. Nakamura, *J. Am. Chem. Soc.*, 2009, **131**, 11949–11963; (*c*) T. Yamagami, R. Shintani, E. Shirakawa and T. Hayashi, *Org. Lett.*, 2007, **9**, 1045–1048.

11 (*a*) C. M. Guisan, F. Tato, E. Bunuel, P. Calle and D. J. Cardenas, *Chem. Sci.*, 2013, **4**, 1098–1104; (*b*) J. A. Przyojski, H. D. Arman and Z. J. Tonzetich, *Organometallics*, 2012, **31**, 3264–3271; (*c*) L. Xiang, J. Xiao and L. Deng, *Organometallics*, 2011, **30**, 2018–2025.

12 (*a*) Y. S. Wang, H. M. Sun, X. P. Tao, Q. Shen and Y. Zhang, *Chin. Sci. Bull.*, 2007, **52**, 3193–3199; (*b*) M. Z. Chen, H. M. Sun, W. F. Li, Z. G. Wang, Q. Shen and Y. Zhang, *J. Organomet. Chem.*, 2006, **691**, 2489–2494.

13 (*a*) X. Li, M. Wang, D. Zheng, K. Han, J. Dong and L. C. Sun, *Energy Environ. Sci.*, 2012, **5**, 8220–8224; (*b*) F. Wang, W. G. Wang, X. J. Wang, H. Y. Wang, C. H. Tung and L. Z. Wu, *Angew. Chem., Int. Ed.*, 2011, **50**, 3193–3197; (*c*) M. L. Singleton, J. H. Reibenspies and M. Y. Darensbourg, *J. Am. Chem. Soc.*, 2010, **132**, 8870–8871.

14 (*a*) S. Zhu, R. Liang, L. Chen, C. Wang, Y. Ren and H. Jiang, *Tetrahedron Lett.*, 2012, **53**, 815–818; (*b*) T. Schaub, M. Backes and U. Radius, *Organometallics*, 2006, **25**, 4196–4206.

15 L. C. Song, C. G. Li, J. H. Ge, Z. Y. Yang, H. T. Wang, J. Zhang and Q. M. Hu, *J. Inorg. Biochem.*, 2008, **102**, 1973–1979.

16 L. C. Song, X. Luo, Y. Z. Wang, B. Gai and Q. M. Hu, *J. Organomet. Chem.*, 2009, **694**, 103–112.

17 J. D. Lawrence, T. B. Rauchfuss and S. R. Wilson, *Inorg. Chem.*, 2002, **41**, 6193–6195.

18 X. Zhao, I. P. Georgakaki, M. L. Miller, J. C. Yarbrough and M. Y. Darensbourg, *J. Am. Chem. Soc.*, 2001, **123**, 9710–9711.
19 P. Buchgraber, L. Toupet and V. Guerchais, *Organometallics*, 2003, **22**, 5144–5147.
20 M. L. Singleton, R. M. Jenkins, C. L. Klemashevich and M. Y. Darensbourg, *C. R. Chimie*, 2008, **11**, 861–874.
21 J. F. Capon, S. Ezzaher, F. Gloaguen, F. Y. Pétillon, P. Schollhammer, J. Talarmin, T. J. Davin, J. E. McGrady and K. W. Muir, *New J. Chem.*, 2007, **31**, 2052–2064.
22 (*a*) T. Liu and M. Y. Darensbourg, *J. Am. Chem. Soc.*, 2007, **129**, 7008–7009; (*b*) J. W. Tye, J. Lee, H. W. Wang, R. R. Mejia, J. H. Reibenspies, M. B. Hall and M. Y. Darensbourg, *Inorg. Chem.*, 2005, **44**, 5550–5552.
23 (*a*) L. C. Song, J. H. Ge, X. G. Zhang, Y. Liu and Q. M. Hu, *Eur. J. Inorg. Chem.*, 2006, 3204–3210; (*b*) L. C. Song, Z. Y. Yang, H. Z. Bian, Y. Liu, H. T. Wang, X. F. Liu and Q. M. Hu, *Organometallics*, 2005, **24**, 6126–6135; (*c*) R. R. Mejia, D. Chong, J. H. Reibenspies, M. P. Soriaga and M. Y. Darensbourg, *J. Am. Chem. Soc.*, 2004, **126**, 12004–12014; (*d*) D. Chong, I. P. Georgakaki, R. R. Mejia, C. J. Sanabria, M. P. Soriaga and M. Y. Darensbourg, *Dalton Trans.*, 2003, 4158–4163.
24 (*a*) B. Li, T. B. Liu, M. L. Singleton and M. Y. Darensbourg, *Inorg. Chem.*, 2009, **48**, 8393–8403; (*b*) T. B. Liu, B. Li, M. L. Singleton, M. B. Hall and M. Y. Darensbourg, *J. Am. Chem. Soc.*, 2009, **131**, 8296–8307.
25 J. Wang, G. Li, X. Ju, H. Xia, F. Fan, J. Wang, Z. Feng and C. Li, *J. Catal.*, 2013, **301**, 77–82.
26 *CRYSTALCLEAR 1.3.6*, Rigaku and Rigaku/MSC, 9009 New Trail Dr, The Woodlands, TX 77381, USA, 2005.
27 G. M. Sheldrick, *SHELXS-97, A Program for Crystal Structure Solution*, University of Göttingen, Germany, 1997.
28 G. M. Sheldrick, *SHELXL-97, A Program for Crystal Structure Refinement*, University of Göttingen, Germany, 1997.